International Journal of Mass Spectrometry 462 (2021) 116515

Contents lists available at ScienceDirect

International Journal of Mass Spectrometry

journal homepage: www.elsevier.com/locate/ijms

A chemical dynamics study of the HCl + HCl^+ reaction

Yuheng Luo [a], Thomas Kreuscher [b], Christopher Kang [a], William L. Hase [c, 1], Karl-Michael Weitzel [b, **], Rui Sun [a, *]

[a] Department of Chemistry, The University of Hawai'i at Manoa, Honolulu, HI, 96822, USA
[b] Fachbereich Chemie, Physikalische Chemie, Philipps Universität Marburg, Marburg, Germany
[c] Department of Chemistry and Biochemistry, Texas Tech University, Lubbock, TX, 79409, USA

ARTICLE INFO

Article history:
Received 24 November 2020
Received in revised form
21 December 2020
Accepted 22 December 2020
Available online 5 January 2021

ABSTRACT

A recent guided ion beam study of the HCl + HCl^+ reaction has revealed two different products [*Phys. Chem. Chem. Phys.* **2015**, *17* (25), 16454–16461]. The first is the proton transfer product, H_2Cl^+ + Cl, where the cross section of the reactions associated with this product, as predicted, monotonically decreases as the collision energy between the product increases. The second is the product HCl^+ + HCl, where the cross section of the reaction shows a local maximum at the collision energy of 0.5 eV. The nature of this unusual behavior of the cross section is not clear. In this manuscript, state of the art *ab initio* molecular dynamics (AIMD) simulation is performed to study this bimolecular collision of HCl^+ + HCl. The potential energy of profile of this system is first characterized with high-level *ab initio* methods, and then a computationally efficient method is selected for AIMD simulation. The cross sections from AIMD agree well with those from the experiments for both products. The AIMD trajectories reveal the complexity of this seemingly-simple reaction – a total of five different pathways that result in the aforementioned two products. The simulation also sheds light on the mystery of the local maximum of the cross section regarding the HCl^+ + HCl product.

1. Introduction

Charge transfer and proton transfer reactions represent the most fundamental reactions in the field of ion molecule chemistry. At the same time, they are among the most efficient reactions in nature. For the symmetric charge transfer reaction $^{36}Ar^+ + Ar$, cross sections as high as 80 $Å^2$ have been measured at a center of mass collision energy of 0.2 eV [1]. For the proton transfer reaction $H_2^+ + H_2 \rightarrow H_3^+ + H$, cross sections as high as 1000 $Å^2$ have been reported at a collision energy of 0.5 meV [2]. In fact the cross sections reported by Allmendinger et al. are fully compatible with Langevin calculations for the reaction of a charge mono pole with a polarizable target [3]. Together with data from Glenewinkel-Meyer et al. [4], the reaction system $H_2^+ + H_2 \rightarrow H_3^+ + H$ now represents one of the best documented examples for Langevin characteristics obeyed over a wide range of collision energies. On the other hand, since the early studies, many ion molecule reactions have been reported to exhibit cross sections significantly lower than the Langevin limit [5]. The situation becomes even more complex when considering reactions of an ion with a dipolar target. In that case the cross section is in general predicted to be above the Langevin limit [6]. Again, there are numerous examples reporting cross sections well below the approximate dipole orientation (ADO) and below the Langevin limit [7,8].

Reaching a topical level of understanding today requires the combination of state-of-the-art experiment and theory. For anion-molecule reactions a high level of sophistication has been reached by combined experimental and theoretical studies for several examples [9,10]. For cation-molecule reactions, we have only recently reached the possibility to compare high level molecular dynamics calculations on an *ab initio* potential energy surface with guided ion beam experiments [11–15]. In this manuscript, we present an extensive *ab initio* molecular dynamics (AIMD) study of the dynamics of the reaction system HCl^+ + HCl that yields two products: the proton transfer one (PT, forming H_2Cl^+ + Cl) and the charge transfer one (CT, forming HCl + HCl^+). Particular emphasis is given to the variation of reaction dynamics with respect to the center of mass collision energy.

* Corresponding author.
** Corresponding author.
E-mail addresses: weitzel@chemie.uni-marburg.de (K.-M. Weitzel), ruisun@hawaii.edu (R. Sun).
[1] Dr. William L. Hase passed away on Mar 23rd, 2020.

https://doi.org/10.1016/j.ijms.2020.116515
1387-3806/

In a recent study, Uhlemann et al. [7] have investigated the dynamics of this reaction with a guided ion beam experiment. Their research has shown that the absolute cross sections for PT (and deuteron transfer) decrease with the increase of center of mass collision energy, E_{col}. The cross section for CT (and $DCl^+ + HCl$) exhibits a maximum with $E_{col} = 0.5$ eV. Uhlemann et al. [7] also investigated the impact of rotational angular momentum of the ion (HCl^+/DCl^+) on the dynamics of the reaction, and reported that the cross section for PT decrease significantly with increasing rotational angular momentum ion before increasing again for the highest value investigated. The impact of rotational angular momentum on the dynamics of the CT reaction is less clear and highly dependent on the collision energy. Although a simple model in which both the collision energy and part of the rotational energy are available for the reaction was employed to rationalize the experiments [7], the exact dynamics of this reaction remains largely unknown.

Quantum chemistry calculation has been an effective method of studying the energy profile of gas phase reaction since its development in the early 1950s [16,17]. In an effort to better understand the experimental results, Uhlemann et al. [7] have utilized high-level *ab initio* method to identify the reaction path of the PT reaction: reactants (i.e. $HCl^+ + HCl$) approach with their H—Cl axis perpendicular to one another and form a pre-reaction complex, $[HCl{-}{-}HCl]^+$, which crosses the transition state (TS) via one H atom rotating into the Cl—Cl axis. A post-reaction complex, $[HClH{-}Cl]^+$ is formed before reaching the product (i.e. $H_2Cl^+ + Cl$). Although the energy profile opens access to chemical information such as reaction rate, time-of-flight of the product, etc., unfortunately, their validity is at the mercy of the presumption that a statistical ensemble is maintained for all intermediates involved [10,18,19]. It requires the lifetime of the intermediates formed after the collision is sufficient for the intramolecular vibrational redistribution (IVR), a situation that is not guaranteed in a highly dynamically system excited through bimolecular collision [20]. For example, many ion-molecule reactions have been reported to contain a significant portion of direct reactions (i.e. without forming any intermediates), barrier recrossings (i.e. many transitions between pre- and post-reaction complexes), and other non-IRC behaviors [15,19,21].

AIMD simulation [22,23] is an ideal computational method to capture the dynamics of the reaction by following the motion of atoms in real time. In AIMD, the interactions between atoms (i.e. energy gradient, corresponding to forces acting on atoms) is directly calculated on-the-fly with *ab initio* methods and their positions are propagated iteratively by solving the classical equations of motions over a small time interval [24]. In this way, the time-evolution of the coordinates of the system (usually referred to as "trajectories") is collected. Further, to accurately model reactions in real life, AIMD simulations of chemical reactions need to sample a statistical ensemble of trajectories corresponding to the conditions of the experiments. Herein, a few thousand AIMD trajectories of this reaction with a low (0.2 eV, 4.6 kcal/mol), medium (0.5 eV, 11.5 kcal/mol), and high (1.0 eV, 23.1 kcal/mol) collision energy are simulated with no rotational excitation of HCl^+. The cross section computed from AIMD simulations are compared with the experiments, and several interesting characteristics of reaction have been revealed. This study lays a solid foundation for future investigation on how the rotational excitation impacts the dynamics of the reaction.

2. Methods

2.1. Potential energy surface

Shown in Fig. 1, the reaction path includes two intermediates connecting with one submerged barrier (i.e. TS-1). The energy

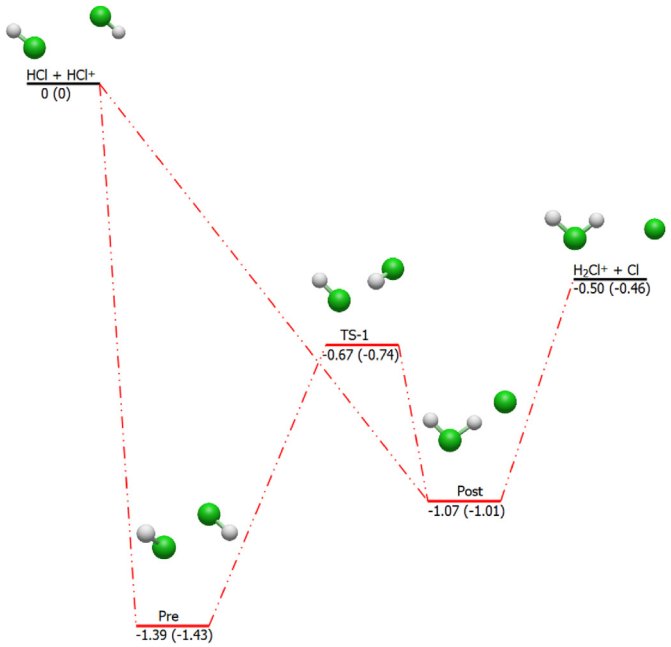

Fig. 1. The potential energy profile of the $HCl^+ + HCl \rightarrow H_2Cl^+ + Cl$ (PT) reaction. The values (in eV) are calculated with MP2/def2-SVP level of theory and the values in parenthesis are calculated with CCSD(T)/CBS//CCSD(T)/cc-pCVDZ. Zero-point energy is included in these values.

profile of this reaction has been first reported by Burda [25] and updated by Uhlemann [7] with second order Møller—Plesset perturbation theory (MP2) [26], coupled-cluster singles and doubles (CCSD) [27], and coupled-cluster singles and doubles plus perturbative triples (CCSD(T)) [28]. According to CCSD(T)/aug-cc-pVTZ [29]//CCSD/def2-TZVPP [30], the heat of the reaction at 0 K is -0.440 eV, somewhat lower than the experimental heat of the reaction, -0.465 eV [31]. Since it is of great importance to obtain an accurate potential energy profile as the benchmark to select optimal *ab initio* method for AIMD in simulating this reaction, several improvements have been made as compared to the previous investigation: (1). Employ CCSD(T) for the geometry optimizations and zero-point energy (ZPE) calculations — previously, CCSD(T) was only used to calculate energy of structures optimized with lower level of theory [7]; (b) Include core-valence correlating functions and weighted core-valence correlating functions to the correlation-consistent polarized valence basis sets (cc-pVXZ) [29] to form correlation-consistent polarized core-valence basis sets (cc-pCVXZ) [32] and weighted correlation-consistent polarized core-valence basis sets (cc-pwCVXZ) [33], respectively — these basic sets are known to accurately represent similar systems; (c) extrapolate the result to the complete basis set (CBS) limit [34]; — the gold standard of *ab initio* calculation. These efforts collectively improve the accuracy and reliability of the benchmark potential energy profile, whose results are summarized in Fig. 1. As shown, the heat of the reaction according to CCSD(T)/CBS//CCSD(T)/cc-pCVDZ is -0.464 eV (-0.466 eV if the ZPEs are scaled by 0.969 for anharmonicity [35]). The excellent agreement between the theoretical and experimental heat of reaction (-0.465 eV) bespeaks for the accuracy of CCSD(T)/CBS//CCSD(T)/cc-pCVDZ in representing the potential energy of this reaction. In addition to improving the accuracy upon previously reported structures in Fig. 1, a new transition state (see TS-2 in Fig. 2) was found and verified by an intrinsic reaction coordinate (IRC) [36—38] calculation. We note that Post-1 and Post-2 are structurally the same as Post in Fig. 1, but they differ in the source of the H in H_2Cl^+ that is closer to the Cl

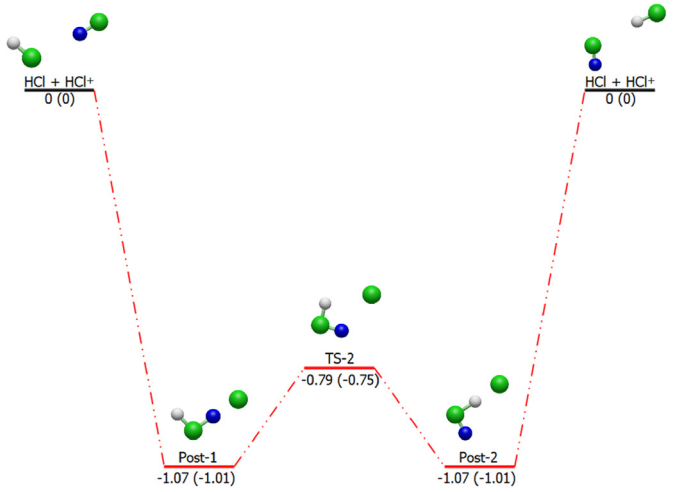

Fig. 2. The potential energy profile of the hydrogen exchange pathway. The H original from the HCl^+ reactant ion is colored blue. The values (in eV) are calculated with MP2/def2-SVP level of theory and the values in parenthesis are calculated with CCSD(T)/CBS//CCSD(T)/cc-pCVDZ. Zero-point energy is included in these values. (For interpretation of the references to color in this figure legend, the reader is referred to the Web version of this article.)

radical (see Fig. 2). This newly-found TS-2 is expected to open up a competing channel to the PT product H_2Cl^++H − the system could have formed the pre-reaction complex, crossed TS-1, and formed the post-reaction complex (Pre → TS-1 → Post in Fig. 1), but instead of forming H_2Cl^++H, it crosses TS-2 and forms Post-2, following the Pre → TS-1 → Post (Post-1) → TS-2 → Post-2 → HCl^+ + HCl. It is of interest to investigate how this additional TS could impact the dynamics of the reaction.

2.2. AIMD simulations

To ensure the conservation of the total energy of the reaction system in a trajectory, the time interval between updating the position of the atoms is usually on the order of one-tenth of a femtosecond [39–41]. A chemical reaction in the gas phase in general takes place on the scale of picoseconds, therefore there are usually a few thousand to tens of thousands of *ab initio* energy gradient calculations involved in modeling each trajectory. Further, to accurately model reactions in real life, AIMD simulations of chemical reactions need to sample a statistical ensemble of (usually a few thousand) trajectories corresponding to the conditions of the experiments, such as various impact parameters (b) and orientations (θ) of the collision [39–41]. Multiplying the number of trajectories with the number of *ab initio* energy gradient calculations per trajectory leads to millions of such calculations and makes the AIMD simulation very computationally demanding. This enormous amount of computation presents an inevitable tradeoff between the accuracy of the *ab initio* method and the ergodicity of the sampling.

In addition to being affordable, the *ab initio* method employed for AIMD needs to represent the potential energy profile of the reaction, i.e., optimizing all the key points (reactants, intermediates, transition states, and products) and calculating their relative energies accurately. In this manuscript, 10 commonly-used density functional theory (DFT) functionals and MP2 combined with various double-zeta, triple-zeta, or effective core potentials (ECP) [42–44] basis sets, a total of 231 affordable candidate methods, have been tested and their relative potential energy profiles are summarized in Table S1 in the Supplementary Information. To evaluate their accuracy in representing the reaction, the root mean square displacement (RMSD) of relative potential energies from each candidate method is computed via the following Eq. (1):

$$RMSD = \sqrt{\frac{1}{N}\sum_{i=1}^{N}\delta_i^2}\ , \delta_i = PE(i) - PE_{ref}(i) \tag{1}$$

where N is the total number of structures on the potential energy surface (see Fig. 1) and δ_i is the difference in relative potential energies between a candidate method (i.e. $PE(i)$) and the benchmark (i.e. $PE_{ref}(i)$, CCSD(T)/CBS//CCSD(T)/cc-pCVDZ) for structure i.

As shown in Table 1, candidate methods with ECP included have seen worse the results compared to those without. Among candidate DFT methods, the M06−2X [45] functional combined with Pople basis sets [46] show the best performance, e.g. M06−2X/6-311G** represents one of the smallest RMSD value. With regard to MP2, its combination with Karlsruhe [30] and augmented correlation-consistent [29] basis sets also shows low RMSD value (e.g. less than 0.1 eV). Several candidate methods of the lowest RMSD, including both DFTs and MP2, are employed to run trial AIMD simulations, and unfortunately, the electron density have been observed to be unstable in trajectories of all DFT candidate methods. For example, while the two reactants are separated, they share the total charge of this system (+0.5 on each reactant) instead of +1 on one and 0 on the other. This behavior takes place in spite of the fact that at the beginning of the AIMD simulation, the charges are correctly assigned. In contrast to that, the MP2 methods combined with Karlsruhe basis sets [30] (def2-SVP, def2-TZVPP, def2-TZVPPD, etc.) demonstrate correct electron density throughout the simulation. With regard to the balance between accuracy and efficiency, MP2 with triple-zeta basis sets is about 5 times slower than it with double-zeta basis sets, while the gain in accuracy is marginal at best (0.003 eV in RMSD). After considering all the aforenoted factors, MP2/def2-SVP is selected as the method for the AIMD simulations in this manuscript.

The initial condition of AIMD simulations is set to represent the guided ion beam experiment of HCl^+ + HCl reaction by Uhlemann et al. [7] The rotational quantum number of reactant ion and reactant molecule are set to 0 and 3, respectively, and the vibrational quantum number of both reactants are set to 0. The two reactants are initially separated by 10 Å, a far enough distance to neglect the intermolecular interaction between them. The initial orientations between the reactants are randomly sampled. The positions of the atoms are propagated by velocity Verlet algorithm in VENUS [47] with a time step of 0.1 fs with the energy gradients calculated by an applicable quantum chemistry method in NWChem [24,48] (in this case, MP2/def2-SVP). The partial charges of each atom are calculated at every integration step with Mulliken population analysis to identify the potential charge transfer trajectories. The trajectories are halted once either the distance between two newly formed products exceeds 10 Å, or they return to reactants after the collision. The reactants are set to collide with a fixed relative translational energy of 0.2, 0.5, or 1.0 eV. For each collision energy, b_{max}, the largest impact parameter, is detected by systematically increasing the impact parameter b until no reactive trajectory is observed. b_{max} is identified as the largest b where at least one trajectory is reactive among 100 trajectories. In the production run, trajectories of $b > b_{max}$ are deemed unnecessary for their low reaction probabilities. In order to account for the correct probability of the collisions, the number of trajectories sampled at each impact parameter is proportional to the impact parameter [15]. In this manuscript, 100 trajectories are sampled at the smallest impact parameter of $b_{min} = 1.0$ Å. As a result, the number of trajectories sampled at a given b, $N(b)$ is computed as:

Table 1
The RMSD of each candidate method with respect to the benchmark value (CCSD(T)/CBS//CCSD(T)/cc-pCVDZ) are summarized in the table. The unit of energy is eV. N/A indicates at least one of the structures on the potential energy profile (Fig. 1) is not found with the corresponding candidate method (see Table S1 in the Supplementary Information).

Basis Set	MP2	DFT Functionals									
		B3LYP	M05	M06	M06−2X	M06-L	XM06	CM06-L	XMVS15	B97	B98
aug-cc-pVDZ	0.07	0.33	0.20	0.22	0.14	0.42	N/A	N/A	0.29	0.35	0.29
aug-cc-pCVDZ	0.07	0.27	0.20	0.22	0.14	0.42	N/A	N/A	0.29	0.35	0.29
aug-cc-pwCVDZ	0.07	0.27	0.19	0.22	0.13	0.42	N/A	N/A	0.29	0.29	0.29
cc-pVDZ	0.12	0.38	0.20	0.31	0.14	0.45	N/A	N/A	0.32	0.40	0.31
cc-pCVDZ	0.12	0.30	0.21	0.23	0.14	0.45	N/A	N/A	0.32	0.39	0.31
cc-pwCVDZ	0.12	0.38	0.21	0.23	0.13	0.45	N/A	N/A	0.32	0.39	0.30
def2-TZVPP	0.05	0.33	0.24	0.20	0.10	0.39	N/A	N/A	0.27	0.28	0.28
def2-TZVP	0.06	0.34	0.24	0.26	0.10	0.39	N/A	N/A	0.27	0.28	0.27
def2-TZVPD	0.06	0.32	0.18	0.20	0.10	0.39	N/A	N/A	0.24	0.27	0.27
def2-SVP	0.05	0.46	0.31	0.41	0.24	0.54	N/A	N/A	0.38	0.48	0.46
def2-SVPD	0.06	0.28	0.21	0.25	0.16	0.46	N/A	N/A	0.27	0.32	0.32
def2-TZVPPD	0.05	0.24	0.23	0.20	0.10	0.39	N/A	N/A	0.24	0.27	0.27
6-31 + g*	0.20	0.32	0.15	0.16	0.05	0.40	N/A	N/A	N/A	0.23	0.22
6-311++g**	0.19	0.31	0.13	N/A	0.04	0.39	N/A	N/A	N/A	0.23	0.22
6-311 + g**	0.19	0.21	0.15	0.17	0.03	0.40	N/A	N/A	0.11	0.23	0.22
6−311g**	0.24	0.18	0.13	0.13	0.01	0.37	N/A	N/A	0.28	0.20	0.19
6−31g**	0.19	0.35	0.16	0.27	0.07	0.40	N/A	N/A	0.13	0.36	0.34
LANL08[a] aug-cc-pVDZ[b]	0.22	0.36	0.33	0.38	0.16	0.48	N/A	N/A	N/A	0.38	0.35
LANL08d[a] aug-cc-pVDZ[b]	0.13	0.22	0.27	0.34	0.14	0.43	N/A	N/A	0.27	0.34	0.24
LANL08[a] cc-pVDZ[b]	0.25	0.38	N/A	0.42	0.16	0.51	N/A	N/A	N/A	0.28	0.27
LANL08d[a] cc-pVDZ[b]	0.16	0.31	0.28	0.34	0.13	0.43	N/A	N/A	0.28	0.24	0.24

[a] Basis set for Cl.
[b] Basis set for H.

$$N(b) = N(b_{min}) \cdot \frac{b}{b_{min}}; b \leq b_{max} \quad (2)$$

A detailed justification of the AIMD simulation settings could be found in Ref. 15. A total number of 2200, 1600, and 1100 trajectories are simulated for the relative translational energy of 0.2, 0.5, or 1.0 eV, respectively. The total number of *ab initio* energy gradient calculations has exceeded 53 million in this research.

3. Results

3.1. Reaction pathways

The AIMD has revealed five reaction pathways. For clarification, the atoms in the reactants are labelled as $H(1)Cl^+(2)$ and $H(3)Cl(4)$, these pathways are:

$H(1)Cl^+(2) + H(3)Cl(4) \rightarrow H(1)Cl^+(4)H(3) + Cl(2)$ P1, Proton Transfer (PT)

$H(1)Cl^+(2) + H(3)Cl(4) \rightarrow H(1)Cl^+(2)H(3) + Cl(4)$ P2, Hydrogen Abstraction (HA)

$H(1)Cl^+(2) + H(3)Cl(4) \rightarrow H(1)Cl(2) + H(3)Cl^+(4)$ P3, Charge Transfer (CT)

$H(1)Cl^+(2) + H(3)Cl(4) \rightarrow H(3)Cl^+(2) + H(1)Cl(4)$ P4, Hydrogen Exchange (HE)

$H(1)Cl^+(2) + H(3)Cl(4) \rightarrow H(3)Cl(2) + H(1)Cl^+(4)$ P5, HE&CT.

The reaction probability of these pathways is depicted in Fig. 3. The overall reaction probability decreases with the increase in collision energy, nevertheless, at the highest collision energy tested in this manuscript (i.e. 1.0 eV), about half of the collisions are still reactive. This level of reaction probability is much larger compared to other bimolecular collisions of comparable collision energy, such as S_N2 (less than 10%) [21,40,49] and CH radical addition (less than 40%) [41,50]. Fig. 3 also shows that the proton transfer (PT) pathway, P1, makes up an overwhelming majority of the total reactive trajectories, although its ratio decreases as the increase of the collision energy (i.e. from 93.3% to 86.5% as the collision energy increases from 0.2 to 1.0 eV). The charge transfer (CT) pathway, P3, is the second most populated pathway following the collision of $HCl^+ + HCl$, and in contrast to the PT pathway, its probability

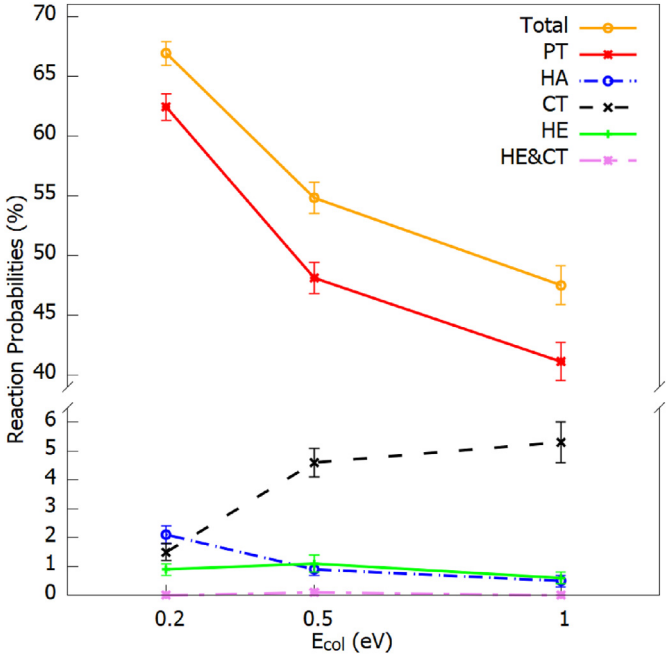

Fig. 3. The reaction probabilities of each pathway vs. the collision energies from the AIMD simulations. The reaction probabilities are calculated from $b_{min} = 1.0$ Å to b_{max}.

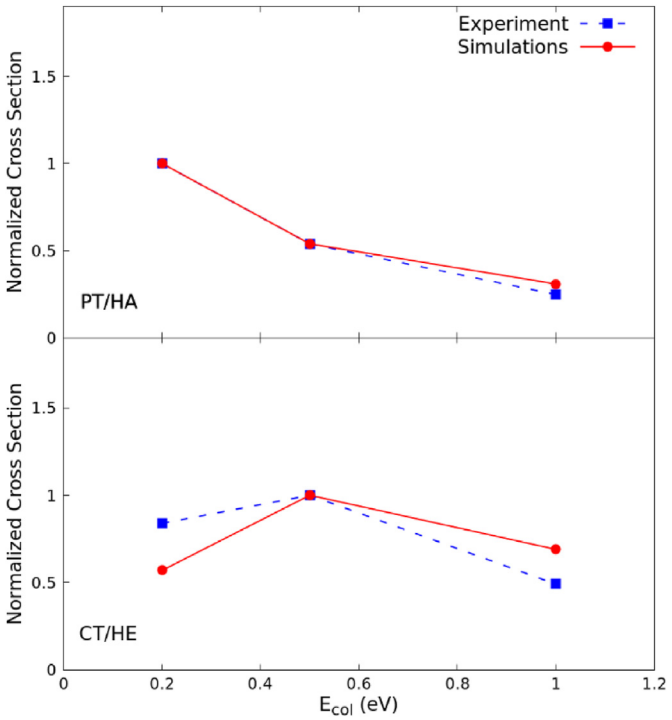

Fig. 4. The normalized cross sections from the AIMD simulations and the experiments. The maximum cross sections of each pathway ($E_{col} = 0.2$ eV of PT/HA and $E_{col} = 0.5$ eV of CT/HE) are scaled to 1.

increases with the increase of collision energy (i.e. from 2.2% to 11.2% as the collision energy increases from 0.2 to 1.0 eV). The reaction mechanism of these two pathways will be discussed in greater details in the following section. In addition, hydrogen abstraction (HA, P2, 1.1−3.1% of the total reaction), hydrogen exchange (HE, P4, 1.3−2.1% of the total reaction), and the combination of HE and CT (P5, 0.0−0.1% of the total reaction), although to a much less degree, have also been observed. One representative animation for each minor reaction pathway is provided in the Supplementary Information. These minor reaction pathways have overall demonstrated to be independent of the collision energy.

3.2. Comparison to guided ion beam experiments

It is essential to validate the results of the AIMD simulations with experiments. As stated in the Introduction, the cross sections of the $HCl^+ + HCl$ reactions have been investigated by Uhlemann et al. [7] at various collision energies and rotationally excited states. It is important to note that according to the guided ion beam experiment, the cross section is measured for all the reactions that lead to $H_2Cl^+ + Cl$, which corresponds to both the PT and the HA pathways observed in the AIMD simulations. In order to observe the charge transfer product, Uhlemann et al. [7] have to employ isotopic substitution for the reactant ion, i.e. $DCl^+ + HCl \rightarrow DCl + HCl^+$, including both CT and HE pathways from the AIMD simulation. Although the electronic potential energy surface is in first approximation identical for both isotopes, the zero-point energy is different. For this reason, we acknowledge that the discrepancy introduced by the isotopes, namely DCl^+ in the guided ion beam experiment and HCl^+ in the AIMD simulations, makes it very challenging to directly compare the results between them, therefore, instead of reproducing values of the experimental cross sections, the focus is to investigate whether the AIMD simulations are able to demonstrate a similar trend of the impact of collision energy on the cross section.

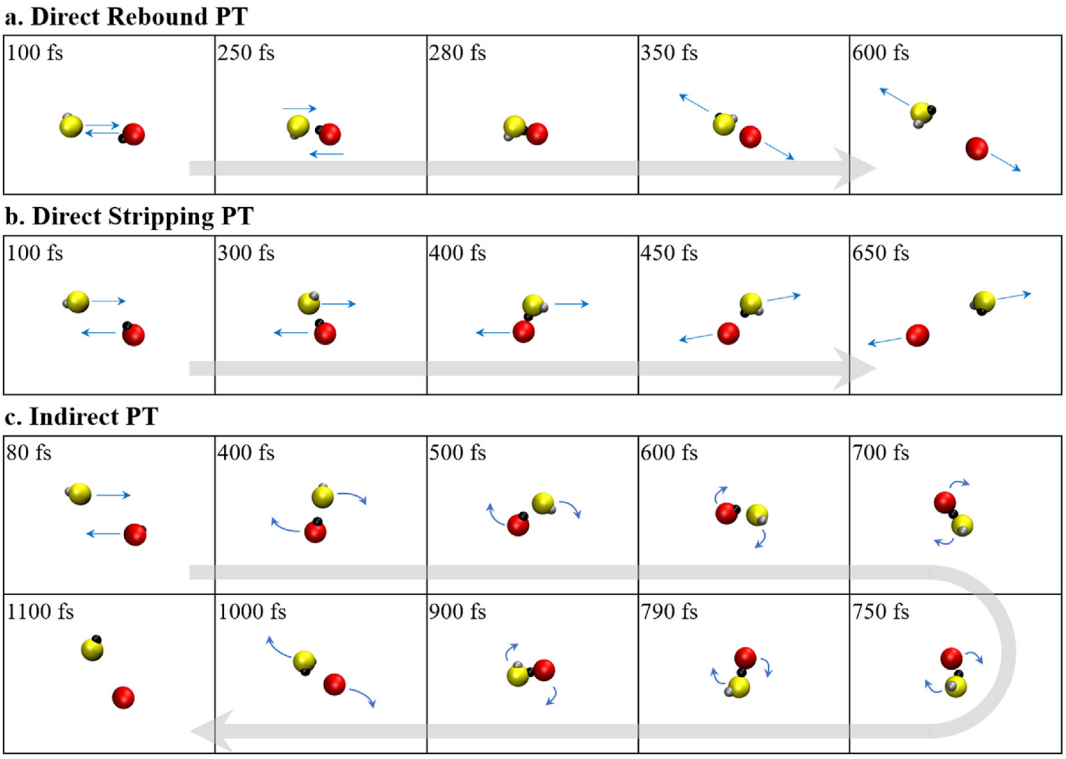

Fig. 5. Snapshots of three representative trajectories of H(black)Cl^+(red) + H(silver)Cl(yellow) → $H_2Cl^+ + Cl$ reaction mechanisms. The blue arrows denote the motions of the molecules and are omitted in the last frame to emphasize that the scattering angle of Ind are isotropic. The bond grey arrows represent the time evolution. (For interpretation of the references to color in this figure legend, the reader is referred to the Web version of this article.)

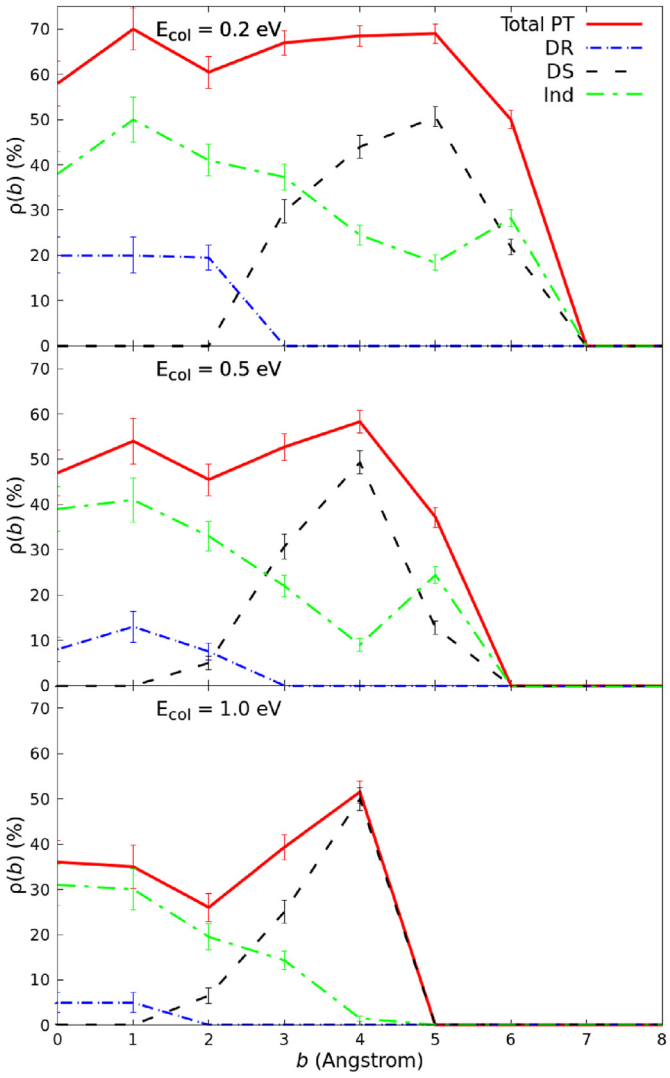

Fig. 6. The reaction probability of PT, $\rho_{PT}(b)$, vs. the impact parameter, b, from the AIMD simulations.

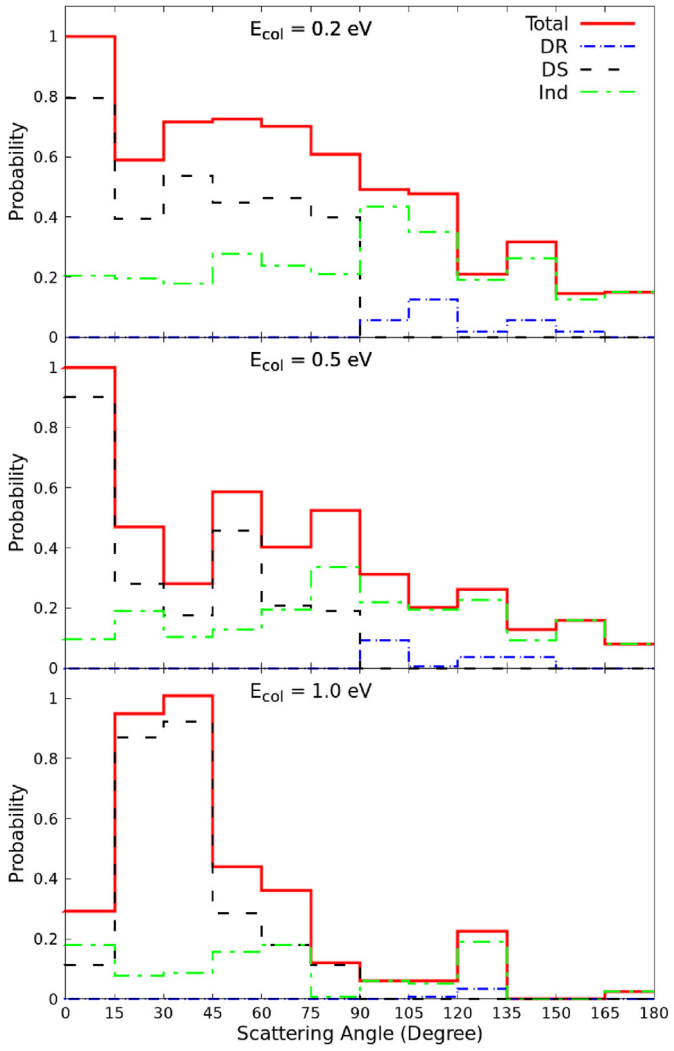

Fig. 7. The scattering angle (defined in the text) distribution from the AIMD simulations. The maximum probability is set to 1.

The cross section (σ) from AIMD simulations is computed with the following equation:

$$\sigma = \int_{b_{min}}^{b_{max}} 2\pi b \cdot \rho(b) \cdot db \tag{3}$$

in which $\rho(b)$ is the reaction probabilities at impact parameter b. As discussed above, the $\rho(b)$ for the $HCl^+ + HCl \rightarrow H_2Cl^+ + Cl$ reaction is the summation of $\rho_{PT}(b)$ and $\rho_{HA}(b)$; while the $\rho(b)$ for the $DCl^+ + HCl \rightarrow DCl + HCl^+$ reaction ($HCl^+ + HCl \rightarrow HCl + HCl^+$ in AIMD simulations) is the summation of $\rho_{CT}(b)$ and $\rho_{HE}(b)$. The cross sections of the $HCl^+ + HCl \rightarrow H_2Cl^+ + Cl$ reaction from AIMD simulations are 85.1 ± 3.2, 46.2 ± 2.6, and 26.1 ± 1.9 Å [2] for E_{col} = 0.2, 0.5, and 1.0 eV, respectively; the cross sections of the $DCl^+ + HCl \rightarrow DCl + HCl^+$ reaction are 3.1 ± 0.8, 5.4 ± 1.1, and 3.7 ± 0.9 Å [2] for E_{col} = 0.2, 0.5, and 1.0 eV, respectively. To highlight the change in the cross section in response to different collision energies, the cross sections for these two reactions are normalized and the results are shown in Fig. 4. As expected for a barrierless reaction (see Fig. 1 for the potential energy profile), the cross sections of the $HCl^+ + HCl \rightarrow H_2Cl^+ + Cl$ (i.e. PT/HA) decrease with increasing collision energies, and the trend of cross section from the AIMD simulations almost matches exactly with the experiment. With regard to the $DCl^+ + HCl \rightarrow DCl + HCl^+$ reaction (i.e. CT/HE), both the guided ion beam experiment and AIMD simulations have shown a maximum in cross section of E_{col} = 0.5 eV, which implies that the collision energy has a non-intuitive impact on this reaction. Overall, the agreement between the AIMD simulations and guided ion beam experiment is remarkable, indicating that the AIMD simulations are able to accurately represent the dynamics of these two reactions.

3.3. The dynamics of the $HCl^+ + HCl \rightarrow H_2Cl^+ + Cl$ reaction

The dynamics of ion-molecule reactions have been investigated over the past decades and various direct and indirect mechanisms have been proposed [10,15,51,52]. Similar to the S_N2 reactions, the $HCl^+ + HCl \rightarrow H_2Cl^+ + Cl$ also demonstrate three mechanisms: direct rebound (DR), direct stripping (DS), and indirect (Ind) mechanisms. Snapshots of each pathway are depicted in Fig. 5. One representative animation for each reaction mechanism is provided in the Supplementary Information. In DR (Fig. 5a), the two reactants move toward each other and the collision is “head-to-head”, with the proton of HCl^+ cation pointing toward the Cl of the HCl

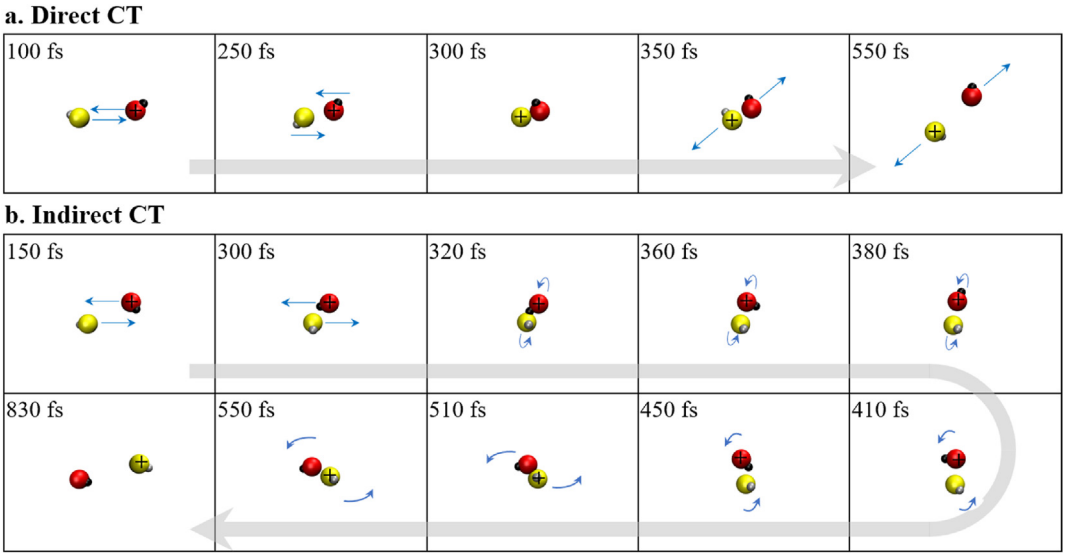

Fig. 8. Snapshots of two representative trajectories of H(black)Cl$^+$(red) + H(silver)Cl(yellow) → HCl + HCl$^+$ reaction mechanisms. The "+" indicate the charge distribution. The blue arrows denote the relative translation of the molecules and are omitted in the last frame to emphasize that the scattering angle of Ind are isotropic. The bond grey arrows represent the time evolution. (For interpretation of the references to color in this figure legend, the reader is referred to the Web version of this article.)

molecule. Immediately after the collision, the proton from HCl$^+$ cation transfers to HCl molecule, forms H_2Cl^+ cation, and bounces off from the point of the collision. In DS (Fig. 5b), while the two reactants approach one another, the HCl$^+$ cation orientate its proton towards the Cl of the HCl molecule. When the distance between the two reactants reaches minimum (i.e. at the point of "passing by"), the proton from HCl$^+$ cation is stripped away by the Cl on HCl and forms H_2Cl^+ cation. Similar to DR, the products (i.e. H_2Cl^+ + Cl) immediately fly off from the collision center. With regard to the Ind (Fig. 5c), the trajectories show a measurable lifetime of the complex formed after collision, which could be trapped into pre- and post-reaction complexes (see Fig. 1) and/or recross the barriers separating them, before eventually dissociating into products.

The reaction probability of the HCl$^+$ + HCl → H_2Cl^+ + Cl reaction versus the impact parameter of the collision b, are shown Fig. 6. We note that 100 trajectories are sampled for b = 0.0 Å to assess its reaction probability, but these trajectories do not contribute to the dynamics of this reaction as suggested by Eq. (2). This figure shows that as the collision energy increases, both the reaction probability at each impact parameter ($\rho(b)$) and the largest impact parameter (b_{max}) decreases. The combination of these two factors accounts for the decrease in the cross section of the reaction as the collision energy increases (see section 3.1 and Fig. 3). The breakdown of the reaction probability of each reaction mechanism is also shown in Fig. 6. Among the three aforementioned reaction mechanisms, DR makes up less than 5% of reactive trajectories for all collision energies; for E_{col} = 0.2 and 0.5 eV, DS and Ind share almost equally the rest 95%; while for E_{col} = 1.0 eV, DS is more than twice as much as the Ind. In accordance with the reaction mechanism observed in Fig. 5, DR trajectories are only observed at small impact parameters (i.e. $b \leq$ 2.0 Å) since the reactants need to be close enough to have a "head-to-head" collision. In contrast, the DS trajectories are only observed at large impact parameters (i.e. $b \geq$ 2.0 Å), which allows for enough distance for the HCl molecule to approach the HCl$^+$ cation from the side and strip away its proton. The Ind trajectories is ubiquitous in all b values as they just require the formation of intermediates after collision, instead of a certain manner of colliding. Fig. 6 also demonstrates that the reaction probability of all three mechanisms decrease as the collision energy increases. In addition, it shows that the dependance of $\rho(b)$ on impact parameter b is very similar for direct mechanisms (DR and DS) at all collision energies. The $\rho_{DR}(b)$ decreases rapidly as the impact parameter gets larger; while $\rho_{DS}(b)$ increases first with the increase of the impact parameter, reaches a maximum with b of 5.0 Å (when E_{col} = 0.2 eV) or 4.0 Å (when E_{col} = 0.5 eV and 1.0 eV). It is interesting to note that the distance between Cl and Cl in the intermediates are ~3.0 Å (2.6 Å for the Pre and 3.2 Å for Post in Fig. 1), respectively, which is slightly smaller than the value of b that sees the largest $\rho_{DS}(b)$. This phenomenon reinforces the fact that although trajectories traverse through the neighboring areas of the intermediates in the phase space, the formation of intermediates is not necessary for the trajectories to be reactive. With regard to the Ind mechanism, its $\rho_{Ind}(b)$ shows a downward trend as the impact parameter increases, however, a local maximum has been found for both E_{col} = 0.2 eV (at b = 6 Å) and 0.5 eV (at b = 5 Å), which is absent in the case of the highest collision energy of E_{col} = 1.0 eV. This is due to the fact that the slower the approach of the reactants (at lower collision energy), the more abundant intramolecular interactions between the reactants are allowed for them to form intermediates and trigger the Ind mechanism. The analysis of the reaction probability of each mechanism has also revealed the reason behind the dip at 2.0 Å of the total reaction probabilities (red curve in Fig. 6) – the reaction probabilities of the DR and Ind mechanisms have decreased but the reaction probabilities of the DS mechanism is still yet to pick up. This dip in the reaction probability at intermediate impact parameter (b ~ 2.0 Å) is absent in almost all the S_N2 bimolecular collisions [21,40,49] but interestingly, is reported in recent studies of bimolecular collision involving a hydrogen halide (HBr^+ + CO_2) [15] and CH radical addition (CH + C_4H_2 and CH + H_2S)[41,50].

The scattering angle (θ) of the HCl$^+$ + HCl → H_2Cl^+ + Cl, defined as the angle between the initial velocity of the reactant molecule (i.e. HCl) the velocity of the product cation (i.e. H_2Cl^+), is also analyzed. As shown in Fig. 7, trajectories of the DR mechanism are backward scattering with obtuse θ(119 ± 17, 113 ± 22, and 125 ± 8° for E_{col} = 0.2, 0.5, and 1.0 eV, respectively). The trajectories of the DS mechanism show forward scattering with acute θ (40 ± 27, 33 ± 27, and 36 ± 17° for E_{col} = 0.2, 0.5, and 1.0 eV, respectively). The θ distribution of Ind trajectories is more or less isotropic, indicating the lifetime of the intermediate is much longer than its rotation

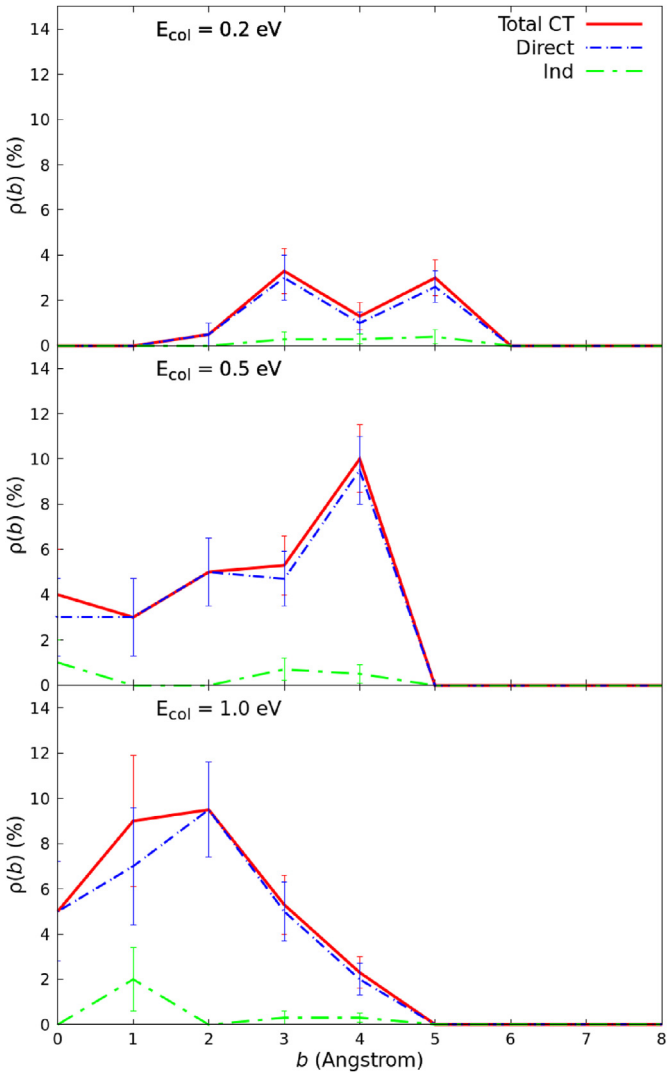

Fig. 9. The reaction probabilities of CT, $\rho_{CT}(b)$, vs. the impact parameter, b, from the AIMD simulations. The reaction probabilities of total CT are summarized in red solid lines. (For interpretation of the references to color in this figure legend, the reader is referred to the Web version of this article.)

period. For example, with E_{col} = 0.2 and 0.5 eV, the ratio between the forward and backward scattering Ind trajectories, (r(forward)/r(backward)), are 0.9 and 1.1, respectively. Nevertheless, for E_{col} = 1.0 eV, this ratio is 2.1, portraying a slight preference to the forward scattering. Trajectories analysis has shown that the average lifetime of the intermediates before dissociating into products are 0.27, 0.19, and 0.16 ps for E_{col} = 0.2, 0.5, and 1.0 eV, respectively. Intuitively, as there is more energy available in the system, the intermediates are more highly excited, thus experiencing shorter lifetime according to Rice–Ramsperger–Kassel–Marcus (RRKM) theory [53].

3.4. The dynamics of the $HCl^+ + HCl \rightarrow HCl + HCl^+$ reaction

As discussed in section 3.2, the cross sections of both the $DCl^+ + HCl \rightarrow DCl + HCl^+$ guided ion beam experiment and the $HCl^+ + HCl \rightarrow HCl + HCl^+$ AIMD simulations (including both CT and HE pathways) have shown a local maximum at E_{col} = 0.5 eV. This is a clear contrast to the behavior of the cross section of the $HCl^+ + HCl \rightarrow H_2Cl^+ + Cl$ reaction, which monotonically decreases with the increase of the collision energy. Between the CT and HE pathways that contribute to the cross section of this reaction in AIMD simulations, CT makes up a much larger portion than HE (see Fig. 3). Further, as shown in Fig. 3, the reaction probability of CT is the only reaction pathway that increases with the increase of the collision energy – a non-intuitive behavior as for reactions that are barrierless, smaller collision energy (i.e. slower approach of reactants) allows for longer time of interactions between molecules, which in general increases the likelihood of the chemical reaction.

Similar to many other ion-molecule reactions, there are direct and indirect mechanisms involved in the trajectories of the CT pathway (snapshots are shown in Fig. 8 and one representative animation for both direct and indirect CT is provided in the Supplementary Information). As depicted in Fig. 9, the reaction probability of the direct mechanism dominates the CT reaction. Trajectory analysis has shown that a successful CT reaction requires a certain orientation between the reactants to ensure that the initial contact is between the chlorine atoms (although, not all collisions initiated by Cl–Cl lead to the CT pathway). Otherwise, the proton on the HCl^+ cation tends to rotate quickly to interact with the chlorine on the HCl molecule and form the $[HClH–Cl]^+$ post-(PT)reaction complex (see Fig. 1). In other words, as the reactants approach one another, the CT reaction via Cl–Cl interaction is competing against the PT reaction via the formation of post-reaction complex. Recall that the reactants are not highly rotationally excited (rotation quantum number is 0 for the ion and 3 for the molecule), and their orientations are randomly sampled. Therefore, a portion of the trajectories would naturally result in Cl–Cl being the initial contact of the collision. However, trajectories of the lowest collision energy of 0.2 eV have shown that the slow approaching of the reactants allows enough time for the positively charged proton from HCl^+ to rotate and bond with the Cl (carrying a negative partial charge) from HCl as the reactant approaches. See Fig. 10a for the snapshot of a representative trajectory. This figure indicates that some of the would-be-CT trajectories are snatched away by the formation of the post-reaction complex and become PT trajectories instead. To highlight the impact of the collision energy, the same trajectory (same initial orientation, vibration, and rotation of the reactants) is reinitiated with a collision energy 0.5 eV and the snapshots are shown in Fig. 10b, in which the approach of the reactants is fast enough to let the Cl–Cl contact first before the proton from HCl^+ has enough time to rotate and interact with the Cl from HCl. The animations of Fig. 10 are provided in the Supplementary Information. The same trajectory with a collision energy of 1.0 eV shows a similar behavior as the one in Fig. 10b.

Therefore, the trajectory analysis seems to have revealed the mystery involved in the increase of the CT pathway probability with respect to the collision energy (see. Fig. 3). The faster approach of the reactants (i.e. the higher the collision energy) overcomes the propensity of rotation of HCl^+ that forms the post-reaction complex and forces a Cl–Cl collision that might lead to the CT pathway. However, it is important to acknowledge that the higher the collision energy is, the shorter interaction time between reactants is allowed, which should in return hinder the reaction probability. These two effects take place simultaneously and compete with one another: at E_{col} = 0.2 eV, the first effect overweighs the second, but the situation is the opposite for E_{col} = 1.0 eV. The trajectories for E_{col} = 0.5 eV demonstrate an optimal speed of approach that is fast enough to minimize the formation of the post-reaction complex (i.e. forcing Cl–Cl collision instead) which would lead to a PT reaction, and slow enough for adequate interaction between reactants.

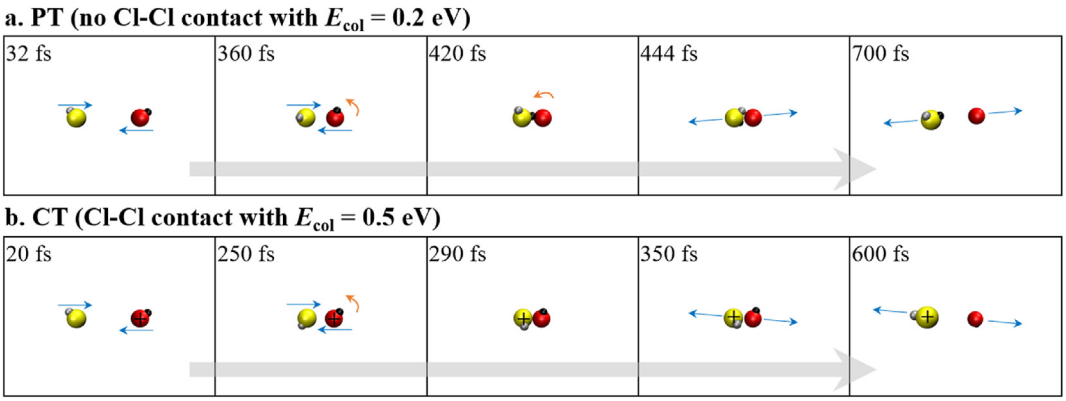

Fig. 10. Snapshots of two trajectories calculated with same initial conditions except collision energies. The "+" indicate the charge distribution of CT trajectories. The blue arrows denote the relative translation of the molecules. The orange arrows denote the relative rotation of HCl^+. The bond grey arrows represent the time evolution. (For interpretation of the references to color in this figure legend, the reader is referred to the Web version of this article.)

4. Discussions

The AIMD simulations of the $HCl^+ + HCl$ reaction revealed various reaction pathways and represented the impact of the collision energy on this reaction in remarkable agreement with the guided ion beam experiment [7]. The simulations also shed light on the mysterious experimental result of the charge transfer reaction, $HCl^+ + HCl \rightarrow HCl + HCl^+$. Intuitively, for a barrier-less reaction (which is the case of the charge transfer reaction), a higher collision energy reduces the reaction probability as there is less time for the reactants to interact with one another [9,10,15,40,49]. The AIMD trajectories show that this trend is observed for all pathways except the charge transfer reaction, which increases with the increase of the collision energy (see Fig. 3). Although the guided ion beam experiment did not provide information of the reaction probability at each impact parameter, it reported that the cross section of the charge transfer reaction (integrated overall possible impact parameters) demonstrates a maximum at E_{col} = 0.5 eV (among 0.2, 0.5, and 1.0 eV, see Fig. 4), which is also verified by the AIMD trajectories. The remarkable agreement between the experiment and AIMD simulation on this non-intuitive behavior of the cross section demonstrates the validity of the trajectories thus analyzing the animations of trajectories is merited.

The animations of the charge transfer trajectories show that Cl—Cl initiated collision (versus H—Cl or H—H initiated collision) is a *necessary but not sufficient condition* for the charge transfer reaction to take place. Since the orientation of the reactions are randomly sampled (see Section 2.2), naturally, a same portion of those trajectories would result in Cl—Cl initiated collisions despite different collision energies. However, the trajectories suggest that when HCl^+ and HCl approach each other, due to Columbic interaction, the proton on HCl^+ tends to interact with the negatively charged Cl on HCl. As a result, those would-have-been Cl—Cl initiated collisions are converted to H(from HCl^+)-Cl(from HCl) initiated collisions, should the Columbic interaction be strong and long-last enough. We note that although the strength of the Columbic interaction only depends on the configuration of the system (i.e. independent of the collision energy), a larger collision energy would reduce the time allowed for the Columbic interaction to convert those would-have-been Cl—Cl initiated collisions to H—Cl initiated collision. In other word, more Cl—Cl initiated collisions are preserved, through which the charge transfer reaction could take place.

Therefore, through decreasing the temporal length of intermolecular interaction, the increase in collision energy has two effects *specifically* in the $HCl + HCl^+$ reaction:

1. Decreasing the reaction probability.
2. Preserving the Cl—Cl initiated collisions, which increases the reaction probability of the charge transfer reaction.

These two effects obviously work against one another, and a detailed breakdown on their relative importance is still under investigation. However, both experiment and simulation suggest that under either of the two extreme conditions, the charge transfer reactions are not likely to take place. At low collision energy (i.e. 0.2 eV), effect #1 is diminished but almost all of those would-have-been Cl—Cl initiated collisions are converted to H—Cl collisions, resulting in low charge transfer reaction probability. At high collision energy (i.e. 1.0 eV), all would-have-been Cl—Cl initiated collisions are preserved, but there is not enough interaction time for the charge transfer reaction to take place. Somewhere in between these two extreme conditions, there exists an optimal condition that maximizes the charge transfer reaction probability.

This discovery, however, seems to be suggesting a contradicting viewpoint to the common knowledge that different isotopes have same chemical property. In other words, $HCl^+ + HCl$ and $DCl^+ + HCl$ should follow the same "chemistry" in forming charge transferred products, i.e. $HCl + HCl^+$ and $DCl + HCl^+$, respectively. However, according to the AIMD simulations, it is reasonable to expect that, replacing H with D in HCl^+ would slow down its rotation (due to a larger moment of inertia) induced by potential energy gradient, thus hinder the impact of collision energy on the orientation of the reactants when they collide. This seems to suggest that the isotope effect does have an impact on this specific reaction. We are currently investigating the dynamics of the collision of the $DCl^+ + HCl$ to fully unravel the isotope effect.

CRediT authorship contribution statement

Yuheng Luo: Methodology, Formal analysis, Writing - original draft, Investigation, Visualization. **Thomas Kreuscher:** Investigation. **Christopher Kang:** Visualization. **William L. Hase:** Conceptualization. **Karl-Michael Weitzel:** Conceptualization, Writing - review & editing. **Rui Sun:** Supervision, Writing - original draft.

Declaration of competing interest

The authors declare that they have no known competing financial interests or personal relationships that could have appeared to influence the work reported in this paper.

Acknowledgement

We thank the Information Technology Service (ITS) Cyberinfrastructure from the University of Hawai'i, Manoa, and XSEDE for the computational resources. We are grateful for the financial support from the University of Hawai'i, Manoa.

Appendix A. Supplementary data

Supplementary data to this article can be found online at https://doi.org/10.1016/j.ijms.2020.116515.

References

[1] S.H. Pullins, R.A. Dressier, R. Torrents, D. Gerlich, Guided-ion beam measurements of Ar+ + Ar symmetric charge-transfer cross sections at ion energies ranging from 0.2 to 300 EV, Zeitschrift fur Phys. Chemie 214 (9) (2000) 1279, https://doi.org/10.1524/zpch.2000.214.9.1279, 36770.
[2] P. Allmendinger, J. Deiglmayr, O. Schullian, K. Höveler, J.A. Agner, H. Schmutz, F. Merkt, New method to study ion–molecule reactions at low temperatures and application to the H2++H2→H3++H reaction, ChemPhysChem 17 (22) (2016) 3596–3608, https://doi.org/10.1002/cphc.201600828.
[3] C. Sanz-Sanz, A. Aguado, O. Roncero, F. Naumkin, Non-adiabatic couplings and dynamics in proton transfer reactions of H n + systems: application to H 2 + H 2 + → H + H 3 + collisions, J. Chem. Phys. 143 (23) (2015) 234303, https://doi.org/10.1063/1.4937138.
[4] T. Glenewinkel-Meyer, D. Gerlich, Single and merged beam studies of the reaction H2+(v = 0, 1; j = 0,4) + H2 -→ H3+ + H, Isr. J. Chem. 37 (4) (1997) 343–352, https://doi.org/10.1002/ijch.199700039.
[5] E.E. Ferguson, Ion-molecule reactions, Annu. Rev. Phys. Chem. 26 (1) (1975) 17–38, https://doi.org/10.1146/annurev.pc.26.100175.000313.
[6] T. Su, E.C.F. Su, M.T. Bowers, Ion–polar molecule collisions. Conservation of angular momentum in the average dipole orientation theory. The AADO theory, J. Chem. Phys. 69 (5) (1978) 2243–2250, https://doi.org/10.1063/1.436783.
[7] T. Uhlemann, J. Wallauer, K.M. Weitzel, Self-reactions in the HCl+ (DCl+) + HCl system: a state-selective investigation of the role of rotation, Phys. Chem. Chem. Phys. 17 (25) (2015) 16454–16461, https://doi.org/10.1039/c5cp02266e.
[8] S. Schmidt, D. Plamper, J. Jekkel, K.-M. Weitzel, Self-reactions in the HBr + (DBr +) + HBr system: a state-selective investigation of the role of rotation, J. Phys. Chem. 124 (41) (2020) 8461–8468, https://doi.org/10.1021/acs.jpca.0c07361.
[9] J. Mikosch, J. Zhang, S. Trippel, C. Eichhorn, R. Otto, R. Sun, W.A. de Jong, M. Weidemüller, W.L. Hase, R. Wester, Indirect dynamics in a highly exoergic substitution reaction, J. Am. Chem. Soc. 135 (11) (2013) 4250–4259, https://doi.org/10.1021/ja308042v.
[10] J. Mikosch, S. Trippel, C. Eichhorn, R. Otto, U. Lourderaj, J.X. Zhang, W.L. Hase, M. Weidemüller, R. Wester, M. Weidemuller, R. Wester, Imaging nucleophilic substitution dynamics, Science (80-.) 319 (5860) (2008) 183–186, https://doi.org/10.1126/science.1150238.
[11] L. Paetow, F. Unger, W. Beichel, G. Frenking, K.-M.M. Weitzel, Rotational dependence of the proton-transfer reaction HBr++CO2→HOCO++Br. I. Energy versus angular momentum effects, J. Chem. Phys. 132 (17) (2010) 174305, https://doi.org/10.1063/1.3409734.
[12] L. Paetow, F. Unger, B. Beutel, K.-M.M. Weitzel, Rotational dependence of the proton-transfer reaction HBr + + CO 2 → HOCO + + Br. II. Comparison of HBr + (2 Π 3/2) and HBr + (2 Π 1/2), J. Chem. Phys. 133 (23) (2010) 234301, https://doi.org/10.1063/1.3515300.
[13] R. Sun, G. Granucci, A.K. Paul, M. Siebert, H.J. Liang, G. Cheong, W.L. Hase, M. Persico, Potential energy surfaces for the HBr + + CO 2 → Br + HOCO + reaction in the HBr + 2 Π 3/2 and 2 Π 1/2 spin-orbit states, J. Chem. Phys. 142 (10) (2015) 104302, https://doi.org/10.1063/1.4913767.
[14] A. Shoji, D. Schanzenbach, R. Merrill, J. Zhang, L. Yang, R. Sun, Theoretical study of the potential energy profile of the HBr + + CO 2 → HOCO + + Br· reaction, J. Phys. Chem. 123 (45) (2019) 9791–9799, https://doi.org/10.1021/acs.jpca.9b07651.
[15] Y. Luo, K. Fujioka, A. Shoji, W.L. Hase, K.-M. Weitzel, R. Sun, Theoretical study of the dynamics of the HBr + + CO 2 → HOCO + + Br reaction, J. Phys. Chem. A 124 (44) (2020) 9119–9127, https://doi.org/10.1021/acs.jpca.0c05323, acs.jpca.0c05323.
[16] R.G. Parr, D.P. Craig, I.G. Ross, Molecular orbital calculations of the lower excited electronic levels of benzene, configuration interaction included, J. Chem. Phys. 18 (12) (1950) 1561–1563, https://doi.org/10.1063/1.1747540.
[17] R. Pariser, R.G. Parr, A semi-empirical theory of the electronic spectra and electronic structure of complex unsaturated molecules, I. *J. Chem. Phys.* 21 (3) (1953) 466–471, https://doi.org/10.1063/1.1698929.
[18] W.L. Hase, D.G. Buckowski, K.N. Swamy, Dynamics of ethyl radical decomposition. 3. Effect of chemical activation vs. Microcanonical sampling, J. Phys. Chem. 87 (15) (1983) 2754–2763, https://doi.org/10.1021/j100238a014.
[19] J.G. López, G. Vayner, U. Lourderaj, S.V. Addepalli, S. Kato, W.A. DeJong, T.L. Windus, W.L. Hase, A direct dynamics trajectory study of F - + CH 3 OOH reactive collisions reveals a major non-IRC reaction path, J. Am. Chem. Soc. 129 (32) (2007) 9976–9985, https://doi.org/10.1021/ja0717360.
[20] J. Zhang, J. Mikosch, S. Trippel, R. Otto, M. Weidemüller, R. Wester, W.L. Hase, F- + CH3I → FCH3 + I- reaction dynamics. Nontraditional atomistic mechanisms and formation of a hydrogen-bonded complex, J. Phys. Chem. Lett. 1 (18) (2010) 2747–2752, https://doi.org/10.1021/jz1010658.
[21] J. Zhang, U. Lourderaj, R. Sun, J. Mikosch, R. Wester, W.L. Hase, Simulation studies of the Cl − + CH 3 I S N 2 nucleophilic substitution reaction: comparison with ion imaging experiments, J. Chem. Phys. 138 (11) (2013) 114309, https://doi.org/10.1063/1.4795495.
[22] S. Pratihar, X. Ma, Z. Homayoon, G.L. Barnes, W.L. Hase, Direct chemical dynamics simulations, J. Am. Chem. Soc. 139 (10) (2017) 3570–3590, https://doi.org/10.1021/jacs.6b12017.
[23] M. Parrinello, Ab initio molecular dynamics, J. Phys. Condens. Matter 14 (1992) 151–156, https://doi.org/10.1007/978-3-642-84713-4_13.
[24] U. Lourderaj, R. Sun, S.C. Kohale, G.L. Barnes, W.A. de Jong, T.L. Windus, W.L. Hase, The VENUS/NWChem software package. Tight coupling between chemical dynamics simulations and electronic structure theory, Comput. Phys. Commun. 185 (3) (2014) 1074–1080, https://doi.org/10.1016/j.cpc.2013.11.011.
[25] J.V. Burda, P. Hobza, R. Zahradník, Properties and reactivity in groups of the periodic system: ion-molecule reactions HX + HX.+ (X = F, Cl, Br, I, At), J. Phys. Chem. 101 (6) (1997) 1134–1139, https://doi.org/10.1021/jp961152c.
[26] C. Møller, M.S. Plesset, Note on an approximation treatment for many-electron systems, Phys. Rev. 46 (7) (1934) 618–622, https://doi.org/10.1103/PhysRev.46.618.
[27] R.J. Bartlett, Coupled-cluster Approach to molecular structure and spectra: a step toward predictive quantum chemistry, J. Phys. Chem. 93 (5) (1989) 1697–1708, https://doi.org/10.1021/j100342a008.
[28] K. Raghavachari, G.W. Trucks, J.A. Pople, M. Head-Gordon, A fifth-order perturbation comparison of electron correlation theories, Chem. Phys. Lett. 157 (6) (1989) 479–483, https://doi.org/10.1016/S0009-2614(89)87395-6.
[29] T.H. Dunning, Gaussian basis sets for use in correlated molecular calculations. I. The atoms boron through neon and hydrogen, J. Chem. Phys. 90 (2) (1989) 1007–1023, https://doi.org/10.1063/1.456153.
[30] F. Weigend, R. Ahlrichs, Balanced basis sets of split valence, triple zeta valence and quadruple zeta valence quality for H to Rn: design and assessment of accuracy, Phys. Chem. Chem. Phys. 7 (18) (2005) 3297, https://doi.org/10.1039/b508541a.
[31] B. Ruscic, R.E. Pinzon, M.L. Morton, G. Von Laszevski, S.J. Bittner, S.G. Nijsure, K.A. Amin, M. Minkoff, A.F. Wagner, Introduction to active thermochemical tables: several "key" enthalpies of formation revisited, J. Phys. Chem. 108 (45) (2004) 9979–9997, https://doi.org/10.1021/jp047912y.
[32] D.E. Woon, T.H. Dunning, Gaussian basis sets for use in correlated molecular calculations. V. Core-valence basis sets for boron through neon, J. Chem. Phys. 103 (11) (1995) 4572–4585, https://doi.org/10.1063/1.470645.
[33] K.A. Peterson, T.H. Dunning, Accurate correlation consistent basis sets for molecular core-valence correlation effects: the second row atoms Al-Ar, and the first row atoms B-Ne revisited, J. Chem. Phys. 117 (23) (2002) 10548–10560, https://doi.org/10.1063/1.1520138.
[34] A.J.C. Varandas, Basis-set extrapolation of the correlation energy, J. Chem. Phys. 113 (20) (2000) 8880–8887, https://doi.org/10.1063/1.1319644.
[35] I.M. Alecu, J. Zheng, Y. Zhao, D.G. Truhlar, Computational thermochemistry: scale factor databases and scale factors for vibrational frequencies obtained from electronic model chemistries, J. Chem. Theor. Comput. 6 (9) (2010) 2872–2887, https://doi.org/10.1021/ct100326h.
[36] K. Fukui, Formulation of the reaction coordinate, J. Phys. Chem. 74 (23) (1970) 4161–4163, https://doi.org/10.1021/j100717a029.
[37] S. Maeda, Y. Harabuchi, Y. Ono, T. Taketsugu, K. Morokuma, Intrinsic reaction coordinate: calculation, bifurcation, and automated search, Int. J. Quant. Chem. 115 (5) (2015) 258–269, https://doi.org/10.1002/qua.24757.
[38] J. Ischtwan, M.A. Collins, Determination of the intrinsic reaction coordinate: comparison of gradient and local quadratic approximation methods, J. Chem. Phys. 89 (5) (1988) 2881–2885, https://doi.org/10.1063/1.454992.
[39] R. Sun, K. Park, W.A. de Jong, H. Lischka, T.L. Windus, W.L. Hase, Direct dynamics simulation of dioxetane formation and decomposition via the singlet ·O–O–CH2–CH2· biradical: non-RRKM dynamics, J. Chem. Phys. 137 (4) (2012) 242–483, https://doi.org/10.1063/1.4736843.
[40] R. Sun, C.J. Davda, J. Zhang, W.L. Hase, Comparison of direct dynamics simulations with different electronic structure methods. F- + CH3I with MP2 and DFT/B97-1, Phys. Chem. Chem. Phys. 17 (4) (2015) 2589–2597, https://doi.org/10.1039/c4cp03589e.
[41] S. Doddipatla, C. He, R.I. Kaiser, Y. Luo, R. Sun, G.R. Galimova, A.M. Mebel, T.J. Millar, A chemical dynamics study on the gas phase formation of thioformaldehyde (H 2 CS) and its thiohydroxycarbene isomer (HCSH), Proc. Natl. Acad. Sci. Unit. States Am. 117 (37) (2020) 22712–22719, https://doi.org/10.1073/pnas.2004881117.
[42] M. Krauss, W.J. Stevens, Effective potentials in molecular quantum chemistry, Annu. Rev. Phys. Chem. 35 (1) (1984) 357–385, https://doi.org/10.1146/annurev.pc.35.100184.002041.
[43] R.B. Ross, S. Gayen, W.C. Ermler, Ab initio relativistic effective potentials with spin–orbit operators. V. Ce through Lu, J. Chem. Phys. 100 (11) (1994) 8145–8155, https://doi.org/10.1063/1.466809.

[44] M. Dolg, X. Cao, Relativistic pseudopotentials: their development and scope of applications, Chem. Rev. 112 (1) (2012) 403−480, https://doi.org/10.1021/cr2001383.
[45] Y. Zhao, D.G. Truhlar, The M06 suite of density functionals for main group thermochemistry, thermochemical kinetics, noncovalent interactions, excited states, and transition elements: two new functionals and systematic testing of four M06-class functionals and 12 other function, Theor. Chem. Acc. 120 (1−3) (2008) 215−241, https://doi.org/10.1007/s00214-007-0310-x.
[46] R. Krishnan, J.S. Binkley, R. Seeger, J.A. Pople, Self-consistent molecular orbital methods. XX. A basis set for correlated wave functions, J. Chem. Phys. 72 (1) (1980) 650−654, https://doi.org/10.1063/1.438955.
[47] X. Hu, W.L. Hase, T. Pirraglia, Vectorization of the general Monte Carlo classical trajectory program VENUS, J. Comput. Chem. 12 (8) (1991) 1014−1024, https://doi.org/10.1002/jcc.540120814.
[48] M. Valiev, E.J. Bylaska, N. Govind, K. Kowalski, T.P. Straatsma, H.J.J. Van Dam, D. Wang, J. Nieplocha, E. Apra, T.L. Windus, W.A. de Jong, NWChem: a comprehensive and scalable open-source solution for large scale molecular simulations, Comput. Phys. Commun. 181 (9) (2010) 1477−1489, https://doi.org/10.1016/j.cpc.2010.04.018.
[49] J. Xie, R. Sun, M.R. Siebert, R. Otto, R. Wester, W.L. Hase, Direct dynamics simulations of the product channels and atomistic mechanisms for the OH- + CH3I reaction. Comparison with experiment, J. Phys. Chem. 117 (32) (2013) 7162−7178, https://doi.org/10.1021/jp4008027.
[50] S.M. Resende, The atmospheric oxidation of the HS radical: reaction with NO2, J. Atmos. Chem. 56 (1) (2006) 21−32, https://doi.org/10.1007/s10874-006-9040-z.
[51] E. Carrascosa, M. Bawart, M. Stei, F. Linden, F. Carelli, J. Meyer, W.D. Geppert, F.A. Gianturco, R. Wester, Nucleophilic substitution with two reactive centers: the CN − + CH 3 I case, J. Chem. Phys. 143 (18) (2015) 184309, https://doi.org/10.1063/1.4934993.
[52] M. Stei, E. Carrascosa, M.A. Kainz, A.H. Kelkar, J. Meyer, I. Szabó, G. Czakó, R. Wester, Influence of the leaving group on the dynamics of a gas-phase SN2 reaction, Nat. Chem. 8 (2) (2016) 151−156, https://doi.org/10.1038/nchem.2400.
[53] F. Di Giacomo, A short account of RRKM theory of unimolecular reactions and of marcus theory of electron transfer in a historical perspective, J. Chem. Educ. 92 (3) (2015) 476−481, https://doi.org/10.1021/ed5001312.